Postural sway in volleyball players

Towards a Population-based approach for dynamic monitoring of underground structures

Camilla Corbani[1], Giulia Delo[2][0000−0003−3502−3045], and Cecilia Surace[1][0000−0002−3993−9432]

[1] Department of Structural, Geotechnical and Building Engineering, Politecnico di Torino, Corso Duca degli Abruzzi, 24, Torino, 10129, Italy
[2] Department of Mechanical and Aerospace Engineering, Politecnico di Torino, Corso Duca degli Abruzzi, 24, Torino, 10129, Italy

Abstract. Underground structures play an increasingly important role in transportation networks and urban areas. Thus, ensuring their structural integrity is essential for safety and operational efficiency. Among the Structural Health Monitoring (SHM) methods already proposed for this type of structure, only a few studies propose vibration-based analyses. Furthermore, data-driven monitoring of infrastructure networks would require the installation of several sensors on each structure, which may be prohibitively expensive for local administrations. The lack of sufficiently large and comprehensive datasets can be addressed through Population-Based Structural Health Monitoring (PBSHM). The PBSHM approach, recently proposed for bridges, wind turbines and aircraft, adopts transfer-learning algorithms to share damage-state knowledge among similar structures and establish a large-scale monitoring system when only a few data are available. This study investigates the potential extension of knowledge sharing to underground structures, such as metro tunnels, by analysing feasible features and damage identification strategies and exploiting the numerical results of two dynamic finite element simulations to provide a domain adaptation case study.

Keywords: Underground Structures · Structural Health Monitoring · Knowledge Transfer · Domain Adaptation

1 Introduction

In recent years, the monitoring of underground structures has gained increasing interest among the scientific community mainly because of the inevitable ageing of structures being in service for decades and the growing number of newly constructed tunnels; therefore, it is essential to adopt an effective and reliable monitoring strategy to ensure structural integrity, operation conditions and users safety. A variety of Structural Health Monitoring (SHM) strategies have already been proposed for underground structures, but most of them focus on static methods, with few investigations on dynamic techniques. Regarding static monitoring, the occurrence of deformations and cracks in tunnel linings have been extensively investigated for both concrete and masonry structures [16], [12], [13],

with also some studies based on *non-contact* strategies, such as in [18], and on machine (and deep) learning methods [17], [14]. Conversely, dynamic monitoring techniques exploit the variation in modal properties, or derived quantities, induced by damages; a tunnel's global stiffness has been evaluated in [20] through a SHM method based on torsional wave speed whereas Feng et al. [7] employed Transmissibility and Cross-correlation functions as damage identification techniques avoiding the problem of measuring the external input. Nevertheless, the close interaction between the tunnel structure and the surrounding soil should be considered to gain a reliable estimate [19].

Furthermore, using data-driven approaches for SHM becomes challenging when exhaustive datasets are missing. This issue can be addressed by the recently introduced Population-Based Structural Health Monitoring (PBSHM) [1]. Traditional SHM techniques are implemented to work on a single structure, and even when machine-learning methods are adopted, the predictive model is updated with the data recorded on that structure. The PBSHM theory overcomes this limitation by relying on information transfer among a population of similar structures, using the known information of one *source* structure to investigate the state of a *target* for which some data are missing. A comprehensive discussion on the PBSHM foundations can be found in [1], [10], and [9], which distinguish *homogeneous* and *heterogeneous* populations based on their similarity. The latter comprises a group of structures with differences in their geometry, materials and/or topology, a variety of transfer-learning methods can be adopted, such as domain adaptation (DA), to harmonise the *source* and *target* features and facilitate data-driven diagnostic inferences. The main assumption behind DA is to transfer information from the source structure to the target ones, even when the distributions of the features are not consistent, by reducing the distance between their domains [8]. Current implementations of this strategy include wind turbines [2], bridges [15], and aerospace structures [4], [6]. Conversely, PBSHM has not yet been applied to underground structures. This work first investigates the feasibility and accuracy of the Transmissibility functions (TFs) and Cross-Correlation Functions (CCFs) as vibration-based damage identification features for underground structures by simulating an integrated tunnel-soil finite element model under two different loading conditions. Subsequently, the model of a second tunnel structure is considered, and a DA algorithm based on Statistic Alignment (SA)[15] is implemented to examine the potentiality of PBSHM for heterogeneous underground structures. The layout of the paper is as follows. Section 2 presents the finite element simulation of the metro tunnels. Section 3 introduces the adopted damage identification strategies. Subsequently, section 4 explores the domain adaptation algorithm used for PBSHM. Lastly, Section 5 presents the discussions and some conclusions.

2 Modelling and Simulation of Metro Tunnel Dynamics

This section presents the numerical simulation of two metro tunnels, adopted to prove the validity of TF and CCF in damage identification and to evaluate

the use of a PBSHM approach, assuming the first structure as a source and the second as a target.

2.1 Finite Element Approach for Tunnel Analysis

The finite element model of the source structure is first introduced. The material properties, geometry and modelling strategy refer to the work of Feng et al. [7]. Accordingly, two finite element models are developed to simulate the healthy and damaged conditions. The models are built in ANSYS software; since the case study regards metro tunnels, their interaction with the ground is considered by developing an integrated tunnel-soil system. The tunnel geometry is shown in Figure 1. The tunnel structure has a circular cross-section of concrete segments, represented by a hollow cylinder. The inner diameter equals 5.5 m, and the outer diameter is 6.2 m, so the wall is 35 cm thick. The longitudinal length is fixed to 168 m, and each tunnel section is discretised with 16 SHELL181 elements 1.2 m long. For what concerns the soil, its average properties around the tunnel structure are considered, as in [7]; to simulate its presence, elements LINK180 and COMBIN14 are respectively used in radial and longitudinal directions, reproducing a full-circle ground spring behaviour. The soil does not show tensile resistance. Thus, LINK180 elements are modelled with compression-only behaviour. Moreover, an elastic modulus of $5.06 \cdot 10^2$ MPa is assigned to LINK180 elements, while a spring constant equal to $3.0 \cdot 10^6$ N/m is applied to COMBIN14; for both LINK180 and COMBIN14, the second edge is fixed. Damage is simulated on a second model by applying a reduction of 13% in the concrete elastic modulus to the 16 shell elements of the sections at a distance $z = 52.8m$ and $z = 54m$ in the longitudinal direction, for a total of 2.4 m of damaged concrete lining. The other material properties, geometry, and assumptions are the same as in the undamaged configuration. All material properties are listed in table 1; in addition, for both models, an equivalent viscous damping of 6% is assigned.

Two additional models were developed to represent the second tunnel in

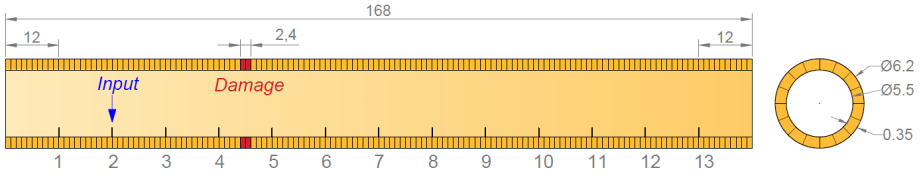

Fig. 1: First tunnel geometry and sensors (measures in m, figure not in scale).

healthy and damaged conditions, following the same assumptions of the first structure. The element discretisation and the soil properties are unchanged, while the geometry and material properties are obtained from [11]: the inner diameter is equal to 5.6 m, the outer one is 6.2 m, so the wall thickness is 30 cm, and a length of 168 m is considered in the longitudinal direction. Thus, the source and target structures share the same topology and type of damage (a re-

Material	**Elastic modulus** [MPa]	**Poisson's ratio**	**Density** $[kg/m^3]$
Concrete	$3.45 \cdot 10^4$	0.2	2551
Damaged concrete	$3.0015 \cdot 10^4$	0.2	2551
Soil	5.00	0.3	1836

Table 1: Concrete and soil properties for the first tunnel structure.

duction of 13% in the concrete elastic modulus) while exhibiting heterogeneous attributes, as discussed in [5]. Table 2 summarises the material properties.

Material	**Elastic modulus** [MPa]	**Poisson's ratio**	**Density** $[kg/m^3]$
Concrete	$3.62 \cdot 10^4$	0.2	2551
Damaged concrete	$3.1494 \cdot 10^4$	0.2	2551
Soil	5.00	0.3	1836

Table 2: Concrete and soil properties for the second tunnel structure.

2.2 Simulation of the Experimental Test Procedure

A hammer impact test is simulated on both models of the first structure to acquire the acceleration responses. Thirteen measurement points are selected at the tunnel bottom with a constant distance of 12 m in the longitudinal direction, as shown in Figure 1. This study proposes two different test procedures to deepen the feasibility assessment of these strategies for tunnel monitoring. In the first one, a vertical impulsive force is applied in a fixed position (point n.2), and the acceleration responses in the vertical direction are gathered for all the sensors; in the second case, the external input is applied sequentially to each section $i+1$, and the acceleration responses are measured only for points i and $i+1$. For both cases, the external input has a duration of 5 ms and an intensity of 4800 N, based on hammer models available for similar applications; a sampling frequency equal to 800 Hz is adopted, whereas the measurement duration is set to 4.5 s. Figure 2 shows two output accelerations in positions 1 and 2 for an external input at location 2.

3 Damage identification strategies and Results

This section provides a brief theoretical description of the two damage identification strategies. Afterwards, their feasibility and accuracy are analysed in the numerical case study. For a viscously damped n-degrees of freedom (DOF) system, the forced vibration problem is ruled by the equation $\mathbf{M}\ddot{\mathbf{x}}(t) + \mathbf{C}\dot{\mathbf{x}}(t) + \mathbf{K}\mathbf{x}(t) = \mathbf{f}(t)$, in which $\mathbf{M}, \mathbf{K}, \mathbf{C}$ are the mass, stiffness and damping matrices respectively, $\mathbf{x}(t)$ is the displacement vector and $\mathbf{f}(t)$ is the load vector. The TF between two DOFs i and j, for the external load applied in the k^{th} DOF is denoted as $T_{ij(k)}$. One benefit of this feature is that it can be calculated without the need to measure the external input or the Frequency Response Function (FRF). The transmissibility damage indicator (TDI) between DOFs i and j, for

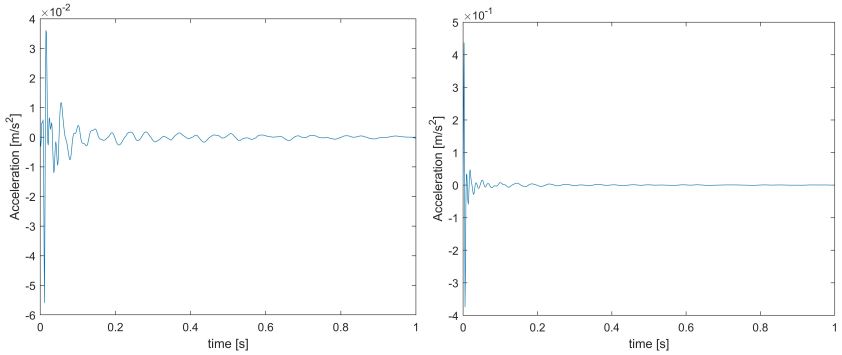

(a) *Measurement point n.1* (b) *Measurement point n.2*

Fig. 2: Acceleration time histories for external input at location 2 in the undamaged model (truncated signals).

the external input applied in k, is defined as:

$$TDI_{ij(k)} = \frac{\int_{\omega_1}^{\omega_2} |\log|T^U_{ij(k)}| - \log|T^D_{ij(k)}|| \, d\omega}{\int_{\omega_1}^{\omega_2} |\log|T^U_{ij(k)}|| \, d\omega} \tag{1}$$

where ω_1 and ω_2 define the frequency range of interest, $T^U_{ij(k)}$ and $T^D_{ij(k)}$ identify the TF for the undamaged and damaged conditions respectively.

Considering the DOFs i and j of the previous n-DOFs system, the CCF can be computed from their acceleration responses $\ddot{x}_i(t)$ and $\ddot{x}_j(t)$ with a time lag τ:

$$R_{i,j}(\tau) = \lim_{T\to\infty} \frac{1}{T} \int_0^T \ddot{x}_i(t)\ddot{x}_j(t+\tau) \, dt \tag{2}$$

The CCF can be normalised with respect to the zero-lag autocorrelation functions. Hence,the cross-correlation damage indicator (CDI) is given by the Equation (3), where superscript U and D denote the normalised CCFs in undamaged and damaged conditions respectively.

$$CDI_{ij} = \frac{\sum_{k_1}^{k_2} ||\widetilde{R}^D_{ij}| - |\widetilde{R}^U_{ij}||}{\sum_{k_1}^{k_2} |\widetilde{R}^U_{ij}|} \tag{3}$$

3.1 Results for Fixed Input Location

The following figures show the results obtained from the fixed input (applied on sensor 2) test, simulated on the first tunnel. Having estimated the natural frequencies of the structure through the FRF plot, for the application of Equation (1) the frequency range 5-40 Hz was chosen, whereas the range of 0.15-0.35 s was used for the CDI. The damage is clearly identified by the TDI between sensors 4-5, where the highest value is reached, as shown in Figure 3. Instead, the CDI fails to accurately identify the damage location, displaying higher values at different pairs of points. Consequently, its validation does not succeed for the fixed input at position 2 within the specified time range.

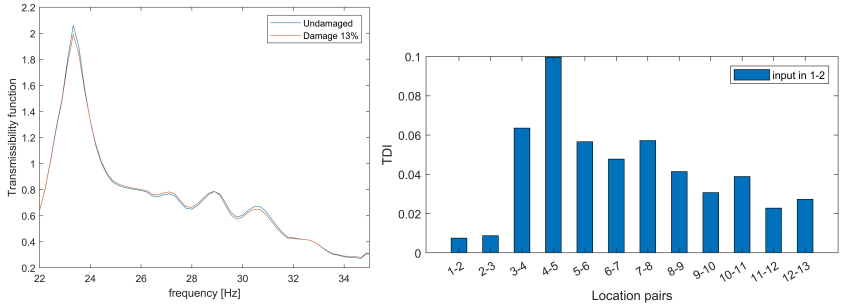

(a) *Transmissibility functions* T_{12}. (b) *TDIs.*

Fig. 3: Transmissibility functions and TDIs for fixed input location in 1-2.

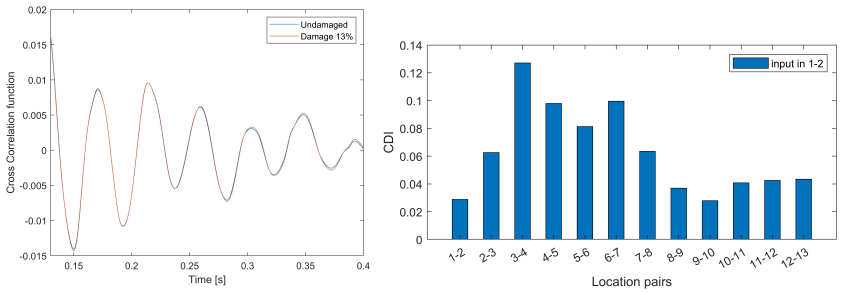

(a) *Cross correlation functions* R_{12}. (b) *CDIs.*

Fig. 4: Cross correlation functions and CDIs for fixed input location in 1-2.

3.2 Results for Variable Input Location

The following figures provide the results found with variable input location (first tunnel); the damage should be detected between pair 4-5. The ranges of interest considered are again 5-40 Hz for the TDI and 0.15-0.35 s for the CDI. As visible in Figures 5 and 6, both damage indicators are capable of correctly localising the damage, showing their higher value at pair 4-5. In addition, by comparing the TF and CCF plots of pairs 1-2 and 4-5, it is distinctly visible that the former presents higher differences between the healthy and damaged conditions because of the closer presence of damage.

3.3 Noise Effects on the Damage-identification Process

Further research on TFs was performed by evaluating their sensitivity to noise for loading condition 2 (mobile input location); this survey is useful to simulate real testing conditions, in which the collected responses are often altered by the presence of noise or random and systematic errors. Thus, the previously stored acceleration measurements are disturbed by applying Gaussian-distributed noise levels equal to 0.1%, 1%, 3%, as in [7]. Figure 7a shows that the TDI damage indicator can successfully identify the damage even in the presence of noise. Similar results are found for the CDI.

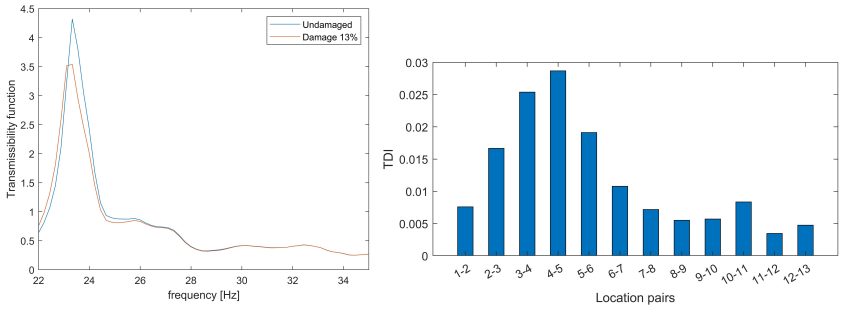

(a) *Transmissibility functions* T_{45}. (b) *TDIs.*

Fig. 5: Transmissibility functions and TDIs for mobile input location.

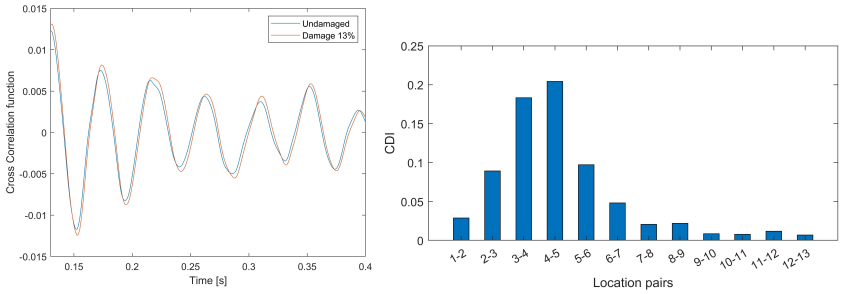

(a) *Cross correlation functions* R_{45}. (b) *CDIs.*

Fig. 6: Cross correlation functions and CDIs for mobile input location.

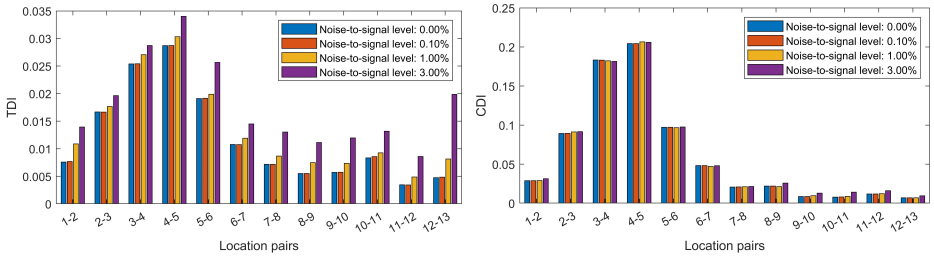

(a) *TDIs.* (b) *CDIs.*

Fig. 7: TDI and CDI for mobile input location under different noise levels.

4 Applying Population-Based SHM to Underground Structures

As these features proved to be sensitive to damage and exhibit generalisable behaviour across similar structures, the current study addresses the possible use of TFs in the PBSHM framework, adopting SA for information transfer between the structures. The use of SA is motivated by the high similarity between

the structures, only differing in some geometrical and material attributes [3]. While the prior analysis only focused on damage localisation based on individual comparisons of transfer functions, the TDI range does not deliver insights on the presence of damage nor the possibility of assessing a threshold for anomaly detection. On the other hand, this task can be tackled by utilising additional knowledge from an appropriate source domain. The analysis is performed assuming a fixed-input setup and selecting $T_{45(2)}$ to address the task of damage detection. The datasets are built via data augmentation employing the previously defined noise-polluted TFs (1% noise-to-signal level).

The SA comprises two methods: the Normal Condition Alignment (NCA) and the Normal Correlation Alignment (NCORAL) [15]. This study implements NCA, which leads to a translation and scaling of the target features to minimise the differences from the source. The source domain includes the features $X_S = \{x_1, x_2, ...x_k\} \in \chi_S$ and their labels Y_S, where $k = 100$ is the total number of samples, evenly split between undamaged ($y = 0$) and damaged ($y = 1$). The training set also includes 25 samples from the target domain, $X_T = \{x_1, x_2, ...x_l\} \in \chi_T$ acquired in undamaged conditions ($y = 0$). Subsequently, a balanced set of 50 samples from the target domain is adopted for testing the algorithm. The NCA calculates the means and standard deviations based on samples that are in undamaged condition.(i.e., $\mu_{s,n}, \sigma_{s,n}$ and $\mu_{t,n}, \sigma_{t,n}$), and applies a transformation to the complete dataset (Equation (4)).

$$z_t^{(j)} = \frac{x_t^{(j)} - \mu_{t,n}}{\sigma_{t,n}} \cdot \sigma_{s,n} + \mu_{s,n} \tag{4}$$

After SA, the TDIs can be computed with reference to the source samples from undamaged conditions. Furthermore, the balanced source dataset allows to compute a threshold, based on Support Vector Machines (SVM), for classifying the test samples. The results of the proposed approach are shown in Figure 8. Additionally, the test results are averaged over 100 repetitions to ensure outcomes robustness.

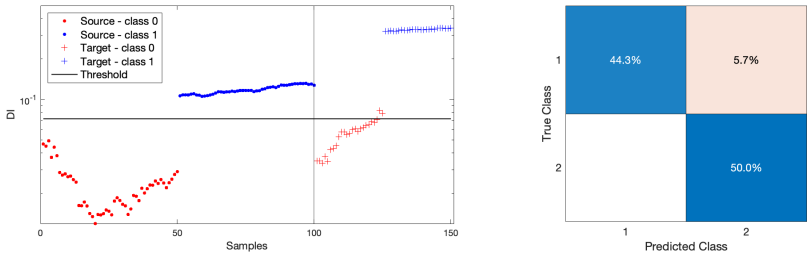

(a) *Damage indicators on the test set.* (b) *Confusion matrix*

Fig. 8: Damage-detection performance on the second metro-tunnel after domain adaptation.

5 Discussion and conclusions

The current study investigates the application of vibration-based and PBSHM methods for monitoring underground structures, exploiting numerical models of two metro tunnels. The hammer impact tests conducted on the finite element model of the first metro tunnel structure proved the sensitivity of TFs and CCFs in localising damage under both loading conditions examined. This sensitivity is evident even under the influence of noise. However, both methods are unable to provide information on the presence of damage, as it is not possible to establish a threshold for distinguishing between healthy and damaged conditions. By considering a second tunnel, the use of TFs has been extended to a PBSHM approach, where a DA algorithm built on SA has been used to minimise the differences between source and target. Hence, damage detection can be carried out on the second tunnel, exploiting the knowledge acquired from the first structure to produce a threshold for classifying the new target samples. The results demonstrate significant performance and robustness, with an acceptable error rate of only 5.7% for incorrectly detected test samples and an overall precision of 94.3%, averaged over 100 repetitions. This study shows how TFs can be relevant not only as sensitive features as vibration-based damage techniques but also in a PBSHM framework for heterogeneous underground structures, paving the way for further insights into this methodology for similar structures.

References

1. Bull, L.A., Gardner, P.A., Gosliga, J., Rogers, T.J., Dervilis, N., Cross, E.J., Papatheou, E., Maguire, A.E., Campos, C., Worden, K.: Foundations of population-based SHM, Part I: Homogeneous populations and forms. Mechanical Systems and Signal Processing **148**, 107141 (2021)
2. Bull, L.A., Gardner, P.A., Rogers, T.J., Dervilis, N., Cross, E.J., Papatheou, E., Maguire, A.E., Campos, C., Worden, K.: Bayesian modelling of multivalued power curves from an operational wind farm. Mechanical Systems and Signal Processing **169**, 108530 (2022)
3. Delo, G., Bunce, A., Cross, E., Gosliga, J., Hester, D., Surace, C., Worden, K., Brennan, D.: When is a bridge not an aeroplane? Part II: A population of real structures. In: European Workshop on Structural Health Monitoring: EWSHM 2022-Volume 2. pp. 965–974. Springer (2022)
4. Delo, G., Roy, R., Worden, K., Surace, C.: Using the inverse finite-element method to harmonise classical modal analysis with fibre-optic strain data for robust population-based structural health monitoring. Strain **e12481** (2024). https://doi.org/10.1111/str.12481
5. Delo, G., Hughes, A.J., Surace, C., Worden, K.: On the influence of attributes for assessing similarity and sharing knowledge in heterogeneous populations of structures. Available at SSRN: http://dx.doi.org/10.2139/ssrn.5006357 (2024)
6. Delo, G., Roy, R., Worden, K., Surace, C.: On the use of the inverse finite element method to enhance knowledge sharing in population-based structural health monitoring. Computers & Structures **307**, 107635 (2025). https://doi.org/10.1016/j.compstruc.2024.107635
7. Feng, L., Yi, X., Zhu, D., Xie, X., Wang, Y.: Damage detection of metro tunnel structure through transmissibility function and cross correlation analysis using lo-

cal excitation and measurement. Mechanical Systems and Signal Processing **60–61**, 59–74 (2015)
8. Gardner, P., Liu, X., Worden, K.: On the application of domain adaptation in structural health monitoring. Mechanical Systems and Signal Processing **138**, 106550 (2020)
9. Gardner, P.A., Bull, L.A., Gosliga, J., Dervilis, N., Worden, K.: Foundations of population-based SHM, Part III: Heterogeneous populations–mapping and transfer. Mechanical Systems and Signal Processing **149**, 107142 (2021)
10. Gosliga, J., Gardner, P.A., Bull, L.A., Dervilis, N., Worden, K.: Foundations of population-based SHM, Part II: Heterogeneous populations–graphs, networks, and communities. Mechanical Systems and Signal Processing **148**, 107144 (2021)
11. Liu, W., Wu, X., Zhang, L., Wang, Y., Teng, J.: Structural health-monitoring and assessment in tunnels: Hybrid simulation approach. Journal of Performance of Constructed Facilities **34**(4) (2020). https://doi.org/10.1061/(asce)cf.1943-5509.0001445
12. Liu, Z., Liu, P., Zhou, C., Huang, Y., Zhang, L.: Structural health monitoring of underground structures in reclamation area using fiber bragg grating sensors. Sensors **19**(13), 2849 (2019). https://doi.org/10.3390/s19132849
13. Mohamad, H., Bennett, P., Soga, K., Mair, R., Bowers, K.: Behaviour of an old masonry tunnel due to tunnelling-induced ground settlement. Géotechnique **60**(12), 927–938 (2010). https://doi.org/10.1680/geot.8.p.074
14. Ouyang, A., Di Murro, V., Cull, M., Cunningham, R., Osborne, J.A., Li, Z.: Automated pixel-level crack monitoring system for large-scale underground infrastructure – a case study at cern. Tunnelling and Underground Space Technology **140**, 105310 (2023). https://doi.org/10.1016/j.tust.2023.105310
15. Poole, J., Gardner, P., Dervilis, N., Bull, L., Worden, K.: On statistic alignment for domain adaptation in structural health monitoring. Structural Health Monitoring **22**(3), 1581–1600 (2023)
16. Wang, X., Wang, M., Jiang, R., Xu, J., Li, B., Wang, X., Yu, J., Su, P., Liu, C., Yang, Q., Lei, M., Liao, X.: Structural deformation monitoring during tunnel construction: a review. Journal of Civil Structural Health Monitoring **14**(3), 591–613 (2023). https://doi.org/10.1007/s13349-023-00741-1
17. Xu, X., Yang, H.: Vision measurement of tunnel structures with robust modelling and deep learning algorithms. Sensors **20**(17), 4945 (2020). https://doi.org/10.3390/s20174945
18. Yang, H., Xu, X.: Structure monitoring and deformation analysis of tunnel structure. Composite Structures **276**, 114565 (2021). https://doi.org/10.1016/j.compstruct.2021.114565
19. Zhou, B., Xie, X.Y., Yang, Y.B., Jiang, J.C.: A novel vibration-based structure health monitoring approach for the shallow buried tunnel. Computer Modeling in Engineering and Sciences **86**(4), 321–348 (2012)
20. Zhou, B., Xie, X., Li, Y.: A structural health assessment method for shield tunnels based on torsional wave speed. Science China Technological Sciences **57**(6), 1109–1120 (2014). https://doi.org/10.1007/s11431-014-5554-9